THE JOURNAL OF PHYSICAL CHEMISTRY C

ARTICLE

pubs.acs.org/JPCC

Charge Transport in a Quantum Dot Supercrystal

Iek-Heng Chu,[†] Marina Radulaski,[‡,∥] Nenad Vukmirovic,[§,∥] Hai-Ping Cheng,[†] and Lin-Wang Wang*[,∥]

[†]Department of Physics and Quantum Theory Project, University of Florida, Gainesville, Florida 32611, United States

[‡]Faculty of Physics, University of Belgrade, Studentski trg 12-15, 11000 Belgrade, Serbia

[§]Scientific Computing Laboratory, Institute of Physics Belgrade, University of Belgrade, Pregrevica 118, 11080 Belgrade, Serbia

[∥]Material Science Division, Lawrence Berkeley National Laboratory, One Cyclotron Road, Mail Stop 66, Berkeley, California 94720, United States

Supporting Information

ABSTRACT: Colloidal semiconductor quantum dots connected by organic or inorganic molecules can form periodic supercrystals. These supercrystals can be used for various types of electronic and optical applications with properties superior to those of random quantum dots and organic polymer mixtures. We have used ab initio calculations to study the charge transport and carrier mobility in such supercrystals. Among the different possible charge transport mechanisms, we found that the phonon-assisted hopping is the most likely mechanism. The calculated carrier mobility agrees well with the experimentally measured results. Our predictions of the size and temperature dependences on the mobility are awaiting experimental confirmation.

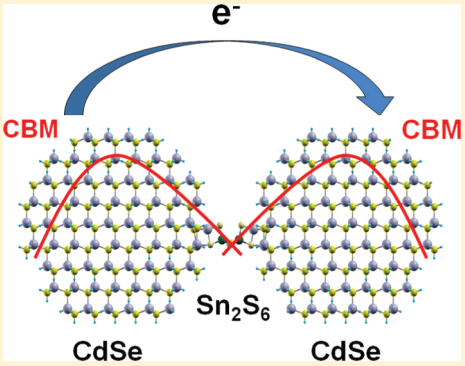

1. INTRODUCTION

Semiconductor colloidal nanostructures have been used in many different applications.[1−7] One type of application is in solar cells[6] and light-emitting diodes,[1,5] where quantum dots or rods were used as light absorbers or light emitters, and also served as electron conducting materials. While most previous applications involve random mixtures of colloidal nanostructures with organic molecules and polymers, there is a current trend to explore the use of the self-assembled quantum dot (QD) arrays. The incredible capability of these QDs to form a periodic crystal structure (supercrystal) provides opportunities to control their electron conductivities and optical properties for designing functional nanostructures.[2,4,8,9] Not only do the QD supercrystals have unique mechanical properties and enhanced thermopower properties,[10] they also have distinctive electrical and optical behaviors.[2] The regular QD arrays (thin films) over nonconducting substrates have demonstrated the field effect transistor (FET) behavior.[11] The QDs can be connected by different linker molecules, and there are experimental efforts[7,9,12,13] to study the electronic effects of these different linker molecules. Nevertheless, the detailed electron transport mechanism has not been established firmly, and there has been little support from theoretical calculations. In this Article, we will study the electron transport in such QD supercrystals using ab initio quality calculations.

There are different possible mechanisms for electron transport inside a QD supercrystal: (a) a narrow bulk band (also called mini-band in the supercrystal) formed by the coupling of nearby QD wave functions and a bulk crystal-like Bloch state electron transport;[14] (b) the tunneling mechanism where the electron transports from one QD to a nearby QD purely by electronic coupling without the help of the phonon;[14−19] (c) over-the-barrier activation mechanism, where electrons are thermally excited to QD eigen-states with energies higher than the potential barrier at the linker, then they transport freely to the other side of the barrier; and (d) the phonon-assisted hopping, where the electron hops from one dot to a nearby dot by absorbing one or multiple phonons.[26] All of these scenarios are schematically depicted in Figure 1. Theoretically speaking, without material-specific, quantitative calculations, all of the above mechanisms are possible. The quantitative calculations are therefore critical for providing qualitative insights into the mechanism of the transport.

To study the electron conductivity in a QD supercrystal, one possible first step is to study the electron transport between two QDs connected by a linker molecule. Such study can also have significance beyond the QD supercrystal, for example, in a random mixture of QDs, where the dot-to-dot connection can still exist. Besides answering the above question about the possible electron transport mechanisms, we will also address the following questions: What is the atomic structure of the QD and linker molecule attachment? How does it affect the charge

Received: July 10, 2011
Revised: September 20, 2011
Published: September 26, 2011

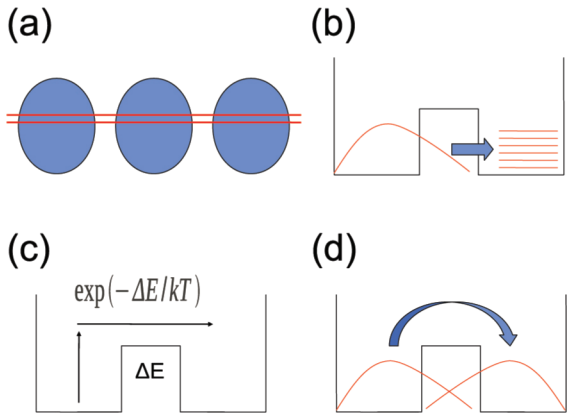

Figure 1. Different possible mechanisms for the electron transport in a QD supercrystal: (a) bulk crystal-like Bloch state electron transport; (b) direct tunneling mechanism without the help of phonon; (c) over-the-barrier activation mechanism; and (d) phonon-assisted hopping.

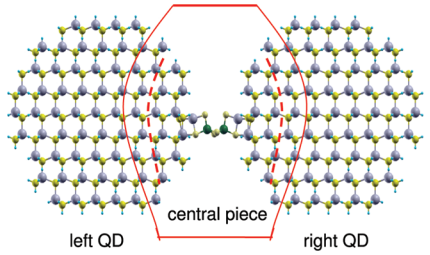

Figure 2. The system with type I attachment contains two 1051-atom CdSe QDs linked by a Sn_2S_6 molecule. The system has been divided into three parts: left and right QDs as well as the central piece. To patch up the charge densities in different parts, a smooth cutoff is introduced at the red dashed line.

transport? What is the effect of QD size on the QD supercrystal conductivity? What is the effect of QD size fluctuation within a supercrystal? What is the temperature dependence for the electron conductivity?

We use the CdSe spherical quantum dots supercrystal linked by metal chalcogenide complexes (MCC), more specifically the Sn_2S_6 molecules, as an example. This system is chosen because such QD supercrystals have been synthesized in laboratories, and strong electron conductivity has been observed.[7,13] We first study two QDs connected by one Sn_2S_6 molecule. The results are then used to study a QD supercrystal. One of the challenges to simulate such a system from first principles calculations is the large size of the system. In experiments, a typical QD is ~5 nm in diameter or consists of about 3000 atoms. Thus, a two-QD system will have about 6000 atoms, which is beyond the limit of current computational power using direct density functional theory (DFT) method.[20,21] To overcome this difficulty, we adopted a multiple level strategy to obtain the total charge density of the two-QD system, as described in the next section. Using this strategy, we are able to study the large system without sacrificing the ab initio accuracy.

2. COMPUTATIONAL METHODS

To obtain the total charge density of the two-QD system in Figure 2 (hence the single particle Kohn−Sham equation under DFT), we use a divide-and-conquer approach. We first cast out a small part of the two-QD system as indicated by the red solid lines in Figure 2. Pseudo hydrogen atoms are used to passivate the cutoff bonds. This subsystem has about 500 atoms, and thus can be calculated self-consistently directly using DFT. We then construct the charge density of each QD (without the surface Sn_2S_6 molecule) using the charge patching method (CPM),[22] which is well-tested[23] with charge density differs from the self-consistent DFT result by only 0.1%. Next, we use a smooth cutoff at the red dashed line in Figure 2 to seamlessly connect the three subsystems (two QDs, and one central region piece) to yield the total charge density of the whole system (see the Supporting Information for details).

Given the total charge density of the system, the DFT potential $V_{tot}(r)$ can be calculated by solving the Poisson equation. The DFT single particle equation is then given as:

$$H\psi_i = \left\{ -\frac{1}{2}\nabla^2 + V_{tot}(r) + \hat{V}_{NL} \right\}\psi_i = \varepsilon_i\psi_i \qquad (1)$$

where the $\hat{V}_{NL}$ is the nonlocal part of the atomic pseudopotentials. In the present work, the folded spectrum method (FSM)[24] is used to calculate the electron conduction band edge states. Instead of working on eq 1, we solve $(H - \varepsilon_{ref})^2\psi_i = (\varepsilon_i - \varepsilon_{ref})^2\psi_i$ where ε_{ref} is the energy reference placed inside the band gap and is close to the conduction band minimum; thus the first few eigen-states are those conduction band edge states of the system. Here, ε_{ref} is evaluated using the generalized moments method (GMM).[25] Note that there is an issue of using DFT eigenenergies to represent the true quasi-particle energies (e.g., a large band gap error). In this work, we are only concerned about the electron conductivity; thus the band gap error will not affect the results significantly. Nevertheless, more accurate GW corrections[26,27] will be used in the future.

3. RESULTS AND DISCUSSION

To study the molecule−QD atomic attachment, we first study the attachment between the Sn_2S_6 molecule and a flat CdSe (10−10) surface. We use this surface to approximate the QD surface. This approximation is reasonable because the (10−10) is the most stable surface of CdSe crystal,[28] and thus it might be the prominent surface of the CdSe QD (note, another prominent surface is the (11−20) surface, which is very similar to the (10−10) surface). Because the molecule attachment only involves a small area on the surface, we thus believe the flat surface attachment and the QD surface attachment can be very similar. Using different initial atomic configurations followed by DFT atomic relaxation to minimize the total energy (see the Supporting Information for calculation details), we find two attachment geometries that have relatively low total energy (large molecule−surface binding energy), as shown in Figure 3. Note that the center Sn−S_2−Sn rhombus has been rotated 90° between these two attachments. While attachment type I has the two end S atoms attached to one standout Cd atom and one neighboring Cd atom in the plane, the attachment type II has these two end S atoms attached to this Cd and another two Cd atoms in the plane. The standout Cd atom is used to satisfy the local electron counting rule. Overall, the attachment type II has a closer distance between the molecule and the surface and is also 0.5 eV lower in energy. Note that it is difficult to claim that the actual molecule−QD attachments in the experiment must be the ones we found in Figure 3. In reality, there could be many different attachments due to local surface environment, thermo fluctuations, and

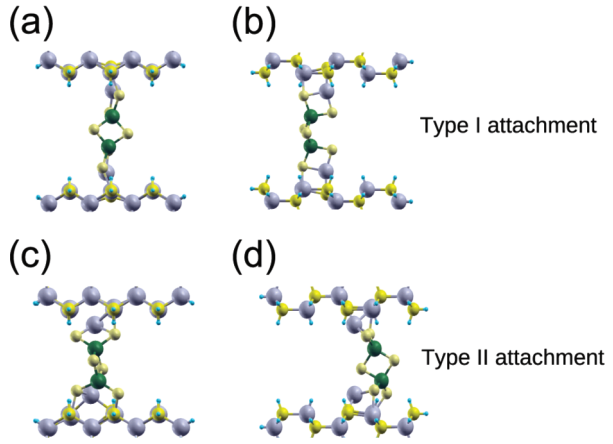

Figure 3. Two types of molecular attachments between Sn_2S_6 and the CdSe surfaces. Panels (a), (b) are the side views of the type I attachment, while panels (c), (d) show the type II attachment at two different views. Here, balls with color yellow, purple, dark green, white, and blue refer to Se, Cd, Sn, S, and H, respectively.

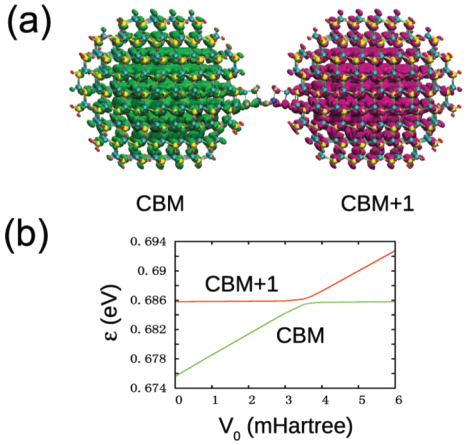

Figure 4. (a) Isosurfaces of the charge densities of CBM (green, left) and CBM+1 (purple, right) electron states. (b) The eigen-energies for CBM and CBM+1 as functions of the added small external potential at one QD, in the case of 1916-atom QDs, type I attachment.

the overall orientation of the QD. Nevertheless, we use the two attachments (one weak, one strong) in Figure 3 to represent the range of plausible attachments in actual experiments.

We then use the atomic configuration of the surface−molecule attachment to construct a two-QD system linked by one Sn_2S_6 molecule. For the other part of the QD surface, we use artificial hydrogen atoms to represent an ideal passivation situation where there is no dangling bond state inside the band gap. The constructed system is shown in Figure 2. According to our calculations, there are two close conduction band states from the two QDs. Typically, one is localized in one QD, while the other is localized in the other QD as shown in Figure 4a. In the experiment,[13] one electron can transfer from one QD state to another QD state, which constitutes the main step of the charge transport. The electronic coupling of these two QD states can be calculated by their anticrossing.[29] This is achieved by artificially adding a very small external potential at one QD, hence driving the energy of that eigen-state crossing the energy of the other

Table 1. Results of the Reorganization Energy λ and Electronic Coupling $V_c(I)$ $[V_c(II)]$ for Type I (II) Molecule Attachment Using Different Sizes of QDs[a]

N	d (nm)	$E_g - E_{g0}$ (eV)	λ (meV)	$V_c(I)$ (meV)	$V_c(II)$ (meV)
468	2.5	1.25	145	4.1	21.9
1051	3.4	0.87	62	1.4	9.5
1916	4.3	0.64	32	0.37	1.9
3193	5.1	0.51	23	0.14	0.48

[a] N is the number of atoms in one QD and d is its diameter. $E_g - E_{g0}$ is the band gap difference between the QD and bulk CdSe, indicating the quantum confinement effect.

eigen-state. This is shown in Figure 4b. The anticrossing is $2V_c$,[30] where V_c is the electron coupling between these two states.

The coupling constants V_c are shown in Table 1 for the two molecular attachments and different QD sizes. There are a few things worth mentioning. First, the coupling constant ranges in a few meV. Note that, if there is no Sn_2S_6 molecule between the two QDs, and the two QDs keep the same distance, the coupling constant will be thousands of times smaller. Second, the coupling constant increases with the decreasing QD size. As the size of the QD decreases from 5.1 to 2.5 nm, the coupling constant increases by a factor of 30 and 45 for the type I and II attachments, respectively. This enhancement is mostly due to the quantum confinement effect. From the 5.1 to 2.5 nm QD, the calculated QD band gap has increased by 0.74 eV. This increase mostly comes from the conduction band, which reduces the relative height of the potential barrier at the Sn_2S_6 molecule, and hence increases the electron coupling. Third, the coupling constant increases from type I attachment to type II attachment by a factor of ∼5, indicating the importance of the atomic structures of the attachments. Not surprisingly, the more tightly bound case (type II attachment) has a larger coupling constant.

To understand the role of phonon in the electron transport, one needs to calculate the electron−phonon coupling. The electron−phonon coupling can be calculated as: $C_{i,j} = \langle \psi_i | \partial H/\partial \mu | \psi_j \rangle$, where μ is the phonon mode, H is the single particle Hamiltonian given in eq 1, and $|\psi_i\rangle$ is the i-th eigen-state of H. The displacement of atomic position under phonon mode μ causes the change of $V_{tot}(r)$ and V_{NL} in H, which induces the electron−phonon coupling. Because the electron wave function as shown in Figure 4a has very small amplitude at the central Sn_2S_6 molecular site, and the small molecule has a small phonon density of state, we can ignore the phonon modes from the molecule. Note that, if one wants to calculate the single phonon transitions caused by a phonon-induced coupling between the "i" and "j" electron states from two neighboring QDs, then it is necessary to include the phonon modes from the linker molecule. In our case, however, the dominant process is the multiphonon process described by the Marcus theory,[31] where the electron−phonon coupling causes a reorganization energy and the electron−electron coupling comes from a state anticrossing picture. In that case, the diagonal electron−phonon coupling constants $C_{i,i}$ and the spring constants of the phonon modes are used to calculate the reorganization energy (the atomic relaxation energy due to the occupation of the electronic state "i"). For this purpose, we can restrict the electron−phonon coupling within each QD. So, the left (right) electron state will only couple to the phonon modes within the left (right) QD. We can thus calculate the electron−phonon coupling inside an isolated QD.

A similar approach is used in a previous calculation for porous Si QDs using a tight-binding model.[32] The direct calculation of $C_{i,j}$ inside one QD is nontrivial as the total number of the possible atomic displacements inside a QD can be close to 10 000. We have approximated this calculation using the CPM.[22] The detail of the calculation is given in the Supporting Information. Figure S1 shows a comparison between the directly calculated electron−phonon couplings for a few atomic displacements using the CPM and the direct self-consistent DFT calculations. We see that the overall CPM error on C_{ij}, especially regarding to the large C_{ij} values, is about 30%, and there is no systematic error. Because the effects of phonon coupling are averaged over thousands of modes, we believe the net error on charge transport can be even smaller.

Under the Marcus theory, what is most important is the reorganization energy. This is the atomic relaxation energy after the electron transfer from one state to another state. As discussed above, this energy can be calculated from the diagonal electron−phonon coupling constant: $C_{i,i}$. More specifically, if $C_{i,i}(R) = \langle\psi_i|\partial H/\partial R|\psi_i\rangle$ is calculated for each atomic coordinate R, then $C_{i,i}(R)$ can be considered as the additional force on each atom R when the electron is removed from (or added on) electron state ψ_i. To compute the atomic relaxation induced by this additional force, we employ the valence force field (VFF) model[33] for quantum dots. Such VFF model can describe the atomic displacement in crystal structures very well. As most of the wave functions (hence the additional atomic forces) are at the interior of the QD, we expect the VFF model should give a good description of the relaxation energy (especially for acoustic phonon modes, as they are most important to be shown in Figure 5). The calculated reorganization energy (note, which is twice the single QD relaxation energy, as the electron moves from one QD to another, inducing relaxations in both QDs) λ is listed in Table 1. Note that λ is roughly inversely proportional to the volume of the quantum dot (see Figure S2) as expected from simple scaling arguments provided in the Supporting Information.

Using the electron coupling constants V_c and the reorganization energies λ given in Table 1, we can employ the Marcus theory formula[31] to calculate the charge transfer rate τ^{-1} from one quantum dot to a neighboring quantum dot:

$$\tau^{-1} = |V_c|^2 \sqrt{\frac{\pi}{\lambda kT\hbar^2}} \exp[-(\lambda + \varepsilon_a - \varepsilon_b)^2/4\lambda kT] \qquad (2)$$

Here, ε_a and ε_b are the electron eigen-energies at the left and the right QD, respectively. If the two quantum dots are exactly the same, they will be the same. However, if there is a quantum dot size fluctuation, then these two eigen-energies can be different. Figure 6 shows the dependence of τ^{-1} as a function of $\varepsilon_a - \varepsilon_b$ for the attachment type I at room temperature. For attachment type II, the curves will be modified by an overall scaling factor proportional to the coupling constant $|V_c|^2$. From Figure 6, we see that the hopping rate changes dramatically at $\varepsilon_a - \varepsilon_b = 0$, from 10^{-3} to 10^{-1} 1/ps, from the largest QD to the smallest QD. Overall, the hopping can happen rather fast, especially for the small QD case. This indicates a high conductivity for the corresponding system.

The above Marcus theory treats the phonon degree of freedom classically within the harmonic approximation and does not allow quantum tunneling of the atomic movement. One can however treat the atomic movement quantum mechanically under harmonic approximations. The corresponding charge

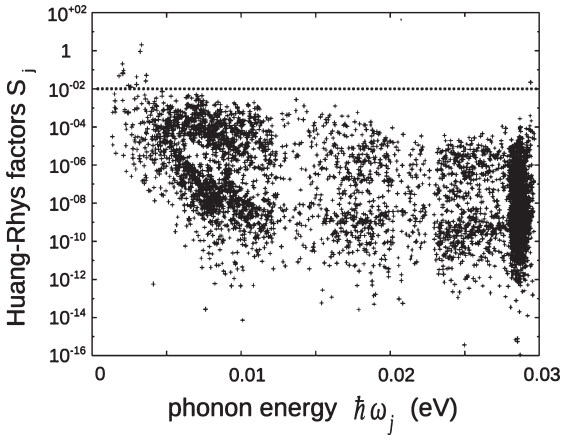

Figure 5. The Huang−Rhys factors S_j for different phonon modes for the $d = 4.3$ nm QD, type I attachment. Each cross represents one phonon mode. There are only a few modes with S_j larger than 0.01, which is indicated by the dashed line.

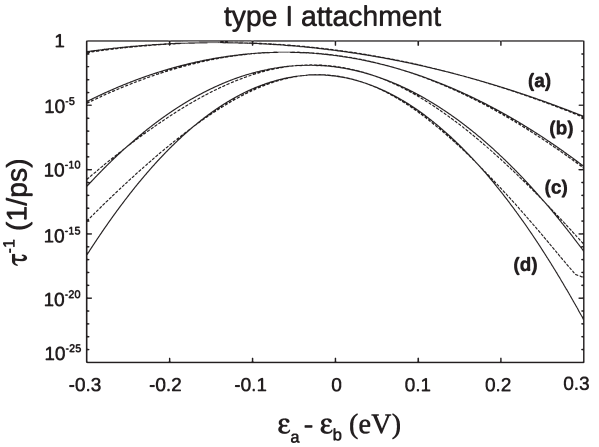

Figure 6. The electron hopping rate τ^{-1} from one QD to another at room temperature as functions of the eigen-energy difference between the two QDs for the cases of (a) 468-atom QD, (b) 1051-atom QD, (c) 1916-atom QD, and (d) 3193-atom QD, type I molecular attachment. Here, solid curves represent the Marcus theory results, while the dashed curves are obtained from the quantum phonon treatment (eq 3).

transfer rate formula is:[34−36]

$$\tau^{-1} = \frac{1}{\hbar^2}|V_c|^2 \int_{-\infty}^{\infty} dt \exp\{i(\varepsilon_a - \varepsilon_b)t/\hbar - \sum_j S_j[(2n_j + 1) - n_j e^{-i\omega_j t} + (n_j + 1)e^{i\omega_j t}]\} \qquad (3)$$

Here, $n_j = 1/[\exp(\hbar\omega_j/k_BT) - 1]$ is the phonon occupation number for phonon mode j at frequency ω_j, $S_j = \lambda_j/\hbar\omega_j$ is the Huang−Rhys factor for the phonon mode ω_j, and λ_j is the reorganization energy for mode ω_j. To calculate λ_j, one first transforms the atomic force $C_{i,i}(R)$ (due to electron−phonon coupling) to the force on phonon mode ω_j, and then calculates the relaxation on each phonon mode as a harmonic oscillator. The calculated Huang−Rhys factors for various phonon modes are shown in Figure 5 for the $d = 4.3$ nm quantum dot. We see

that most of the Huang−Rhys factors are much smaller than 1. Only a few of them approach 1. In general, the largest Huang−Rhys factor concentrates on the few acoustic modes. If we only keep the 14 phonon modes in eq 3 with $S_j > 0.01$ as illustrated by the dashed curve shown in Figure 5, the resulting rate τ^{-1} is very close to the original value including all of the phonon modes. At $\varepsilon_a - \varepsilon_b = 0$, the rate changes only 10%, while at $\varepsilon_a - \varepsilon_b = -0.3$ and 0.3 eV, it decreases by a factor of 10. The latter larger change is due to the fact that for larger $\varepsilon_a - \varepsilon_b$, it will be easier to use the higher frequency phonon modes to satisfy the energy conservations. Thus, those higher frequency modes become more important. For $\varepsilon_a - \varepsilon_b = 0$, even if we only keep the three largest S_j, the result is still good (with an error of 26%). That means the transition rate is controlled by a handful of phonon modes at least near $\varepsilon_a - \varepsilon_b = 0$.

The calculated hopping rates (including all of the phonon modes) using the quantum mechanical formula eq 3 are shown in Figure 6 as the dashed curves. We can see that, overall, there is a remarkable agreement between the Marcus formula result and the quantum mechanical formula result. Near $\varepsilon_a - \varepsilon_b = 0$, the quantum mechanical formula gives slightly larger hopping rates (e.g., 8% for the 4.3 nm diameter QD), as expected from the inclusion of quantum tunneling.

We can now discuss the likelihood of the other transport mechanisms illustrated in Figure 1. Note that the reorganization energies shown in Table 1 are much bigger than the electron coupling constants. This means that an electron prefers to be localized inside a single QD to gain the reorganization energy, instead of being in an extended state to gain the electron coupling energy. As a result, the mini-band picture[14,15] of Figure 1a will not hold.

The model of direct tunneling, Figure 1b, has been used in a few previous works.[7,9,13,14] However, for a direct tunneling to work (without the involvement of the phonon), the other side of the barrier (the electron receiving side) should have a continuous density of states to satisfy the energy conservation law. This is apparently not the case in our system because the other side is also a quantum dot with a few discrete levels (typically 0.1 eV apart) above the CBM. There is, however, a possibility of resonant tunneling. For that to happen, the eigen-energy difference $\varepsilon_a - \varepsilon_b$ must be within the coupling constant V_c. Typically, there are 5% size fluctuations between the QDs. Using the band gap dependence on the QD size shown in Table 1, or previously calculated results,[37] this 5% size distribution roughly corresponds to a 50 meV change in eigen-energy $\varepsilon_{a(b)}$ for the experimentally relevant 4.3, 5.1 nm diameter QD. This is 100 times bigger than the corresponding coupling constant V_c. Thus, it is inappropriate to use any direct tunneling model without involving phonons to describe the charge transfer.

Another picture (Figure 1c) is the direct hopping over the barrier height. Because of thermo fluctuation inside the QD, the electron can jump to a level (a mobile state) inside the QD with its energy above the potential barrier at the molecule. Next, the electron can move from one side to another without the blocking of the potential. The local density of states calculated at the molecule site (Figure S3, S4) indicates that the barrier height relative to the QD conduction band state is about $E_b = 2.4$ eV (for the $d = 5.1$ nm QD). The estimated hopping rate should be: $1/\tau_0 \exp(-E_b/k_BT)$, where $1/\tau_0$ is the transport rate for eigen-states above the barrier height. To have a higher limit of this rate, we can use $1/\tau_0 = \hbar/m_e d^2$ (d is the diameter of the quantum dot). Note in the above formula, τ_0 is the time taken by a free electron in a vacuum to spread from a localized area of size d (with a Gaussian wave function) to a localized area of size $2d$. For $d = 5.1$ nm, we have $\tau_0 = 0.2$ ps. If we take the effective mass of the electron in the conduction band of CdSe, instead of free electron, we have $\tau_0 \approx 0.02$ ps. Given $E_b = 2.4$ eV, we find that even when this maximum $1/\tau_0$ is used, the calculated rate is about 4×10^{-39} ps^{-1}. This value is much smaller than the multiphonon absorption/emission hopping rate described by the Marcus theory as shown in Figure 6. Thus, we can safely ignore this over-the-barrier transport channel. In addition, the temperature dependence for these two pictures is dramatically different. While the over-the-barrier picture has an activation energy of 2.4 eV, the hopping picture within Marcus theory leads to an activation energy of a few tens meV. Temperature-dependent experimental measurements can be performed to verify our prediction.

Table 2. Mobility μ_1 (μ_2) for Type I (II) Molecule Attachment in a QD Supercrystal with $d = 4.3$ nm[a]

5% QD size fluctuation	uniform connection fluctuation	μ_1 (cm^2/V/S)	μ_2 (cm^2/V/S)
no	no	8.22×10^{-2}	2.16
yes	no	4.80×10^{-2}	1.26
yes	yes	1.02×10^{-2}	0.26

[a] The experimental value for the case of 4.5 nm QD array[13] is 3×10^{-2} cm^2/V/S. The Marcus theory is used to describe the transition rate. If the quantum mechanical formula is used, the calculated mobilities will increase for about 5−8%.

From the above discussion, we conclude that the Marcus theory described multiphonon-assisted process is the most likely charge transfer mechanism between the two QDs. Under this picture, we next like to calculate the carrier mobility in a QD supercrystal[38] and to compare the result with the experiment. To do that, we use the second largest quantum dot of 4.3 nm in diameter, which is close to the dot size of 4.5 nm in one experiment.[13] Using a simple cubic QD supercrystal, we calculate the carrier mobilities in the low carrier density limit in three different situations (see the Supporting Information for calculation details): (1) there is no QD size fluctuation; (2) there is 5% QD size fluctuation as described in the experiment; (3) on top of the 5% QD size fluctuation, we assume that the QD−molecule attachment is not as good as described by either type I or type II attachments, and instead there are some loose attachments, which results in a uniform distribution of the electron coupling constant square $|V_c|^2$ varying between 0 and the values listed in Table 1. The 5% size fluctuation leads to an ε_a fluctuation of ∼35 meV described by the $\varepsilon(d)$ curve (fitted to our calculated values) due to quantum confinement effect. However, there is another potential source for the fluctuation of ε_a due to the single particle self-energy. The self-energy term in the GW formalism can be approximated as $1/(\varepsilon_\infty^{\text{eff}} R) - 1/(\varepsilon_\infty^{\text{bulk}} R)$ in a QD,[39] where $\varepsilon_\infty^{\text{bulk}}$ and $\varepsilon_\infty^{\text{eff}}$ are the dielectric constants of the bulk CdSe crystal and effective medium of the QD supercrystal, and R is the QD radius. Judged from the material density of the QD supercrystal, we can assume $\varepsilon_\infty^{\text{eff}} \approx 0.5\varepsilon_\infty^{\text{bulk}} = 3.4$. This self-energy term is then about 0.1 eV for the 4.3 nm diameter QD. As a result, the 5% size fluctuation will introduce an additional 5 meV fluctuation in ε_a, which is however much smaller than the quantum confinement effect fluctuation. The final results after statistical averaging are listed in Table 2. As one can see, when the 5% fluctuation is introduced, the mobility decreases by a factor of 1.7. When the

loose attachment is assumed, the mobility is further reduced by a factor of 5. The calculated mobility agrees rather well with the experimental results if the type I attachment is used. On the other hand, if the type II attachment is used, the calculated mobility can be 10 times larger than the experimental value. Overall, such agreement on the mobility is rather good, as mobility calculation can often differ from experimental results by orders of magnitudes. From our calculation, we can also conclude that, although there might be some type II attachments, the majority of the attachments might be similar to type I like. This is understandable given the complicated situations in the local chemical environments and random QD orientations in the supercrystal. Our result also indicates that between two neighboring QDs, there are probably only a few Sn_2S_6 molecules connecting them, because our one molecule connection result agrees quite well with the experiment.

In the above discussion, we have only considered the hopping from the S-state CBM of one QD to the S-state CBM of another QD. Strictly speaking, however, it is possible for the electron to hop from the S-state of one QD to the P-state (CBM+1) of another QD. The S−P splitting in the QD size range considered here is around 100−150 meV. According to Figure 6, this will lead to 100 or more times reduction in the hopping rate. Thus, unless the size fluctuation is so large as to compensate this energy difference, the S to P transition can be safely ignored. Also, note that we have only calculated the mobility in the low carrier density case using the linear equation method described in the Supporting Information. If the carrier density is high, and state filling and Coulomb blockade effects are strong,[40,41] then Monte Carlo simulations are needed to describe the carrier mobility like the one described in ref 41. The P and even D levels can then become important.[40,41]

The prediction on the quantum dot size dependence for the carrier mobility can be estimated from the hopping rate dependence shown in Figure 6 at $\varepsilon_a = \varepsilon_b$ or be calculated directly from eq 2 using the numbers shown in Table 1. The temperature dependence can also be calculated from eq 2. Because the $\varepsilon_a - \varepsilon_b$ under 5% size distribution is rather similar to λ (or sometimes twice of it), then the temperature dependence for the carrier mobility judged from eq 2 is rather similar to $\exp(-\lambda/kT)$.

4. CONCLUSION

We have investigated the charge transport in a semiconductor QD supercrystal connected by small molecules. We have studied the likelihood of four different possible transport mechanisms: the mini-band bulk Bloch state transport, the direct tunneling, the over-the-barrier thermal transport, and the phonon-assisted hopping. We have identified that the phonon-assisted hopping is responsible for the charge transport in our studied system. We have also discovered that different atomic attachment can play an important role in the charge transport, as does the quantum dot size. With decreasing QD size, the carrier mobility can increase by orders of magnitudes. We have analyzed the effects of QD size fluctuation and the fluctuation of the QD−molecular attachments on the carrier mobility in a QD supercrystal. Finally, from a theoretical point of view, we have examined the validity of the classical Marcus theory using the quantum mechanical treatment for the phonon. We found that Marcus theory is remarkably accurate in this regard. Besides, the phonon-assisted charge hopping is mostly caused by a handful of acoustic phonon modes with the largest Huang−Rhys factors. Our predictions for the QD size and temperature dependence on the supercrystal mobility await experimental confirmation.

■ ASSOCIATED CONTENT

Supporting Information. Details of smooth cutoff for constructing the total charge density, surface−molecule attachment calculations, the electron−phonon couplings, QD size scaling of the reorganization energy, local density of states calculations, and carrier mobility calculation in the QD supercrystal. This material is available free of charge via the Internet at http://pubs.acs.org.

■ AUTHOR INFORMATION

Corresponding Author
*E-mail: lwwang@lbl.gov.

■ ACKNOWLEDGMENT

L.-W.W., N.V., and M.R. are supported by DOE/BES-DE-AC02-05CH11231. I.-H.C. and H.-P.C. are supported by DOE/BES-DE-FG02-02ER45995. N.V. also acknowledges the support from the Serbian Ministry of Science (project ON171017) and the European Commission (FP7 projects PRACE-1IP, HP-SEE and EGI-InSPIRE). This work used the computational resources of the National Energy Research Scientific Computing Center (NERSC) and the National Center for Computational Sciences (NCCS), with the computational time allocated by the Innovative and Novel Computational Impact on Theory and Experiment (INCITE) project, of DOE.

■ REFERENCES

(1) Bulovic, V.; Wood, V.; Panzer, M. J.; Caruge, J. M.; Halpert, J. E.; Bawendi, M. G. *Nano Lett.* **2010**, *10*, 24.
(2) Alivisatos, A. P. *Science* **1996**, *271*, 933.
(3) Harman, T. C.; Taylor, P. J.; Walsh, M. P.; LaForge, B. E. *Science* **2002**, *297*, 2229.
(4) Konstantatos, G.; Howard, I.; Fischer, A.; Hoogland, S.; Clifford, J.; Klem, E.; Levina, L.; Sargent, E. H. *Nature* **2006**, *442*, 180.
(5) Ginger, D. S.; Greenham, N. C. *J. Appl. Phys.* **2000**, *87*, 1361.
(6) Gur, I.; Fromer, N. A.; Geier, M. L.; Alivisatos, A. P. *Science* **2005**, *310*, 462.
(7) Talapin, D. V.; L., J. S.; Kovalenko, M. V.; Shevchenko, E. V. *Chem. Rev.* **2010**, *110*, 389.
(8) Talapin, D. V.; Murray, C. B. *Science* **2005**, *310*, 86.
(9) Yu, D.; Wang, C. J.; Guyot-Sionnest, P. *Science* **2003**, *300*, 1277.
(10) Wang, R. Y.; Feser, J. P.; Lee, J. S.; Talapin, D. V.; Segalman, R.; Majumdar, A. *Nano Lett.* **2008**, *8*, 2283.
(11) Ahn, J. S.; Lee, J. J.; Hyung, G. W.; Kim, Y. K.; Yang, H. *J. Phys. D: Appl. Phys.* **2010**, *43*, 275102.
(12) Jarosz, M. V.; Porter, V. J.; Fisher, B. R.; Kastner, M. A.; Bawendi, M. G. *Phys. Rev. B* **2004**, *70*, 195327.
(13) Kovalenko, M. V.; Scheele, M.; Talapin, D. V. *Science* **2009**, *324*, 1417.
(14) Vanmaekelbergh, D.; Liljeroth, P. *Chem. Soc. Rev.* **2005**, *34*, 299.
(15) Beloborodov, I. S.; Lopatin, A. V.; Vinokur, V. M.; Efetov, K. B. *Rev. Mod. Phys.* **2007**, *79*, 469.
(16) Wang, Y.; Zhang, J.; Zhang, X. G.; Cheng, H. P.; Han, X. F. *Phys. Rev. B* **2010**, *82*, 054405.
(17) Datta, S. *Electronic Transport in Mesoscopic Systems*; Cambridge University Press: Cambridge, 1995.
(18) Ventra, M. D. *Electrical Transport in Nanoscale Systems*; Cambridge University Press: Cambridge, 2008.

(19) Liu, Y.; Gibbs, M.; Puthussery, J.; Gaik, S.; Ihly, R.; Hillhouse, H. W.; Law, M. *Nano Lett.* **2010**, *10*, 1960.
(20) Kohn, W.; Sham, L. J. *Phys. Rev.* **1965**, *140*, 1133.
(21) Hohenberg, P.; Kohn, W. *Phys. Rev. B* **1964**, *136*, B864.
(22) Wang, L. W. *Phys. Rev. B* **2002**, *65*, 153410.
(23) Wang, L. W. *Annu. Rev. Phys. Chem.* **2010**, *61*, 19.
(24) Wang, L. W.; Zunger, A. *J. Chem. Phys.* **1993**, *100*, 2394.
(25) Wang, L. W. *Phys. Rev. B* **1994**, *49*, 10154.
(26) Hedin, L. *Phys. Rev.* **1965**, *139*, A796.
(27) Louie, M. S. H. a. S. G. *Phys. Rev. B* **1986**, *34*, 5390.
(28) Manna, L.; Wang, L. W.; Cingolani, R.; Alivisatos, A. P. *J. Phys. Chem. B* **2005**, *109*, 6183.
(29) Shan, W.; Walukiewicz, W.; Ager, J. W.; Haller, E. E.; Geisz, J. F.; Friedman, D. J.; Olson, J. M.; Kurtz, S. R. *Phys. Rev. Lett.* **1999**, *82*, 1221.
(30) Coropceanu, V.; Cornil, J.; da Silva, D. A.; Olivier, Y.; Silbey, R.; Bredas, J. L. *Chem. Rev.* **2007**, *107*, 926.
(31) Marcus, R. A. *Rev. Mod. Phys.* **1993**, *65*, 599.
(32) Lampin, E.; Delerue, C.; Lannoo, M.; Allan, G. *Phys. Rev. B* **1998**, *58*, 12044.
(33) Keating, P. *Phys. Rev.* **1966**, *145*, 637.
(34) Huang, K.; Rhys, A. *Proc. R. Soc.* **1950**, *204*, 406.
(35) Lax, M. *J. Chem. Phys.* **1952**, *20*, 1752.
(36) Nan, G. J.; Yang, X. D.; Wang, L. J.; Shuai, Z. G.; Zhao, Y. *Phys. Rev. B* **2009**, *79*, 115203.
(37) Li, J. B.; Wang, L. W. *Phys. Rev. B* **2005**, *72*, 125325.
(38) Vukmirovic, N.; Wang, L. W. *Nano Lett.* **2009**, *9*, 3996.
(39) Wang, L. W. *J. Phys. Chem. B* **2005**, *109*, 23330.
(40) Benchorin, M.; Moller, F.; Koch, F.; Schirmacher, W.; Eberhard, M. *Phys. Rev. B* **1995**, *51*, 2199.
(41) Chandler, R. E.; Houtepen, A. J.; Nelson, J.; Vanmaekelbergh, D. *Phys. Rev. B* **2007**, *75*, 085325.

Supplementary information for: Charge transport in a quantum dot supercrystal

Iek-Heng Chu[(1)], Marina Radulaski[(2,4)] , Nenad Vukmirovic[(3,4)], Hai-Ping Cheng[(1)], Lin-Wang Wang[(4)]

(1) Department of Physics and Quantum Theory Project, University of Florida, Gainesville, FL 32611

(2) Faculty of Physics, University of Belgrade, Studentski trg 12-15, 11000 Belgrade, Serbia

(3) Scientific Computing Laboratory, Institute of Physics Belgrade, University of Belgrade, Pregrevica 118, 11080 Belgrade, Serbia

(4) Material Science Division, Lawrence Berkeley National Laboratory, One Cyclotron Road, Mail Stop 66, Berkeley, CA 94720

Email: lwwang@lbl.gov

(1) The smooth cut-off of the charge density and the patch up of the three pieces in Figure 2:

The charge densities in the quantum dot part (both the left and right pieces) as well as the molecule part (the central piece), as illustrated in Figure 2, are computed individually. To patch them up for the total charge density, a mask function $w(\vec{r})$ is introduced which varies smoothly from 0 to 1 when $\vec{r}$ crosses the dashed line in Figure 2 from the quantum dot side to the central molecule side. More specifically, $w(\vec{r}) = 1/(e^{a(d-b)}+1)$, otherwise $w(\vec{r})$ is 0 in the quantum dot part and 1 in the molecule part. Here, $d = |\vec{r} - \vec{r}_{dash}|$ is the shortest distance between $\vec{r}$ and the red dashed line. In the calculations, *a* and *b* are taken as 12.8Å^{-1} and 0.469Å, respectively. The result is insensitive to the exact values of a and b. The total charge density is then calculated as $\rho(\vec{r}) = w(\vec{r})\rho_{center}(\vec{r}) + (1 - w(\vec{r}))\rho_{QD}(\vec{r})$. It is worth mentioning that in order to yield the correct total charge, one might need to rescale the center charge density $\rho_{center}(\vec{r})$ very slightly.

(2) The details of the surface molecule attachment calculations:

The attachment between the molecule Sn_2S_6 and a flat CdSe (1010) surface is modeled by a three-layer slab adsorbed with the molecules. An orthorhombic supercell with dimension of 14.69 x 12.72 x 33.03 $Å^3$ is used in the calculations, in which the slab is periodic in the *x*-*y* plane with a 10 Å vacuum region along the *z* direction. The separation between the neighboring molecules is 10 Å so that the interactions between the molecules can be neglected. The total energy minimizations were performed using density functional theory (DFT)[1, 2] in local density approximation[3], as implemented in the plane-wave based VASP code[4, 5]. Ultrasoft pseudopotentials[6] with a kinetic energy cutoff of 400eV were used to ensure the total energy convergence. Several initial molecule attachment configurations are tested, followed by atomic relaxations. The two lowest energy attachments after the atomic relaxations are shown in Figure 3.

(3) Electron-phonon coupling:

The electron-phonon coupling is calculated by the charge patching method. There are two terms in the single particle Hamiltonian derivative $\partial H / \partial \vec{R}$. The first term is the change of the nonlocal potential in Eq.(1), which is calculated using the conventional method as in a total energy plane wave code. The second term is the change of the local potential, especially the Hartree potential. This is due to two parts; one is the displacement of the nuclei charge, which is represented by the local part of the pseudopotential. Another part is due to the change of valence electron charge density, and consequently the change of the Hartree potential. We have used the CPM[7] to calculate the change of the charge density when an atom is moved. Note, only the charge motifs near the atom $\vec{R}$ need to be changed. This makes the method extremely efficient. This method has been used to calculate the electron-phonon coupling in organic polymer systems[8-10]. Here, in inorganic nanocrystals, we found that it is necessary to screen the long range part of the potential change $\Delta V(\vec{r})$ due to the atomic displacement at $\vec{R}$. This is because, in CPM, the charge density is not calculated self-consistently; as a result, the long range electric field is not screened. We have thus multiplied a fixed spherical screening function $f(|\vec{r}-\vec{R}|)$ on top of $\Delta V(\vec{r})$ (caused by a single atom displacement at $\vec{R}$), here $f(x)$ is a function which is close to 1 when *x* is near zero, and roughly 1/ε when *x* is large, and ε is

the bulk dielectric constant. In practice, the $f(x)$'s for Cd displacement and Se displacement are also different. We obtain this mask function from bulk system calculations where direct DFT calculations have been carried out. $f(x)$ is computed as the ratio of the $\Delta V(\vec{r})$ obtained from CPM and DFT methods. We then use this mask function in the calculation of quantum dot systems.

After $f(x)$ is multiplied to the local potential change $\Delta V(\vec{r})$, we can now calculate the electron-phonon coupling constants: $C_{i,j}(\vec{R}) = \langle \psi_i | \partial H / \partial \vec{R} | \psi_j \rangle$. The results are shown in Figure S1 for the smallest quantum dot where the $\partial H / \partial \vec{R}$ can also be calculated directly from self-consistent DFT calculations. About 20 *i* and *j* are used. One can see that the overall CPM error is probably about 30% especially when the largest electron-phonon couplings are considered. Furthermore, there is no systematic error.

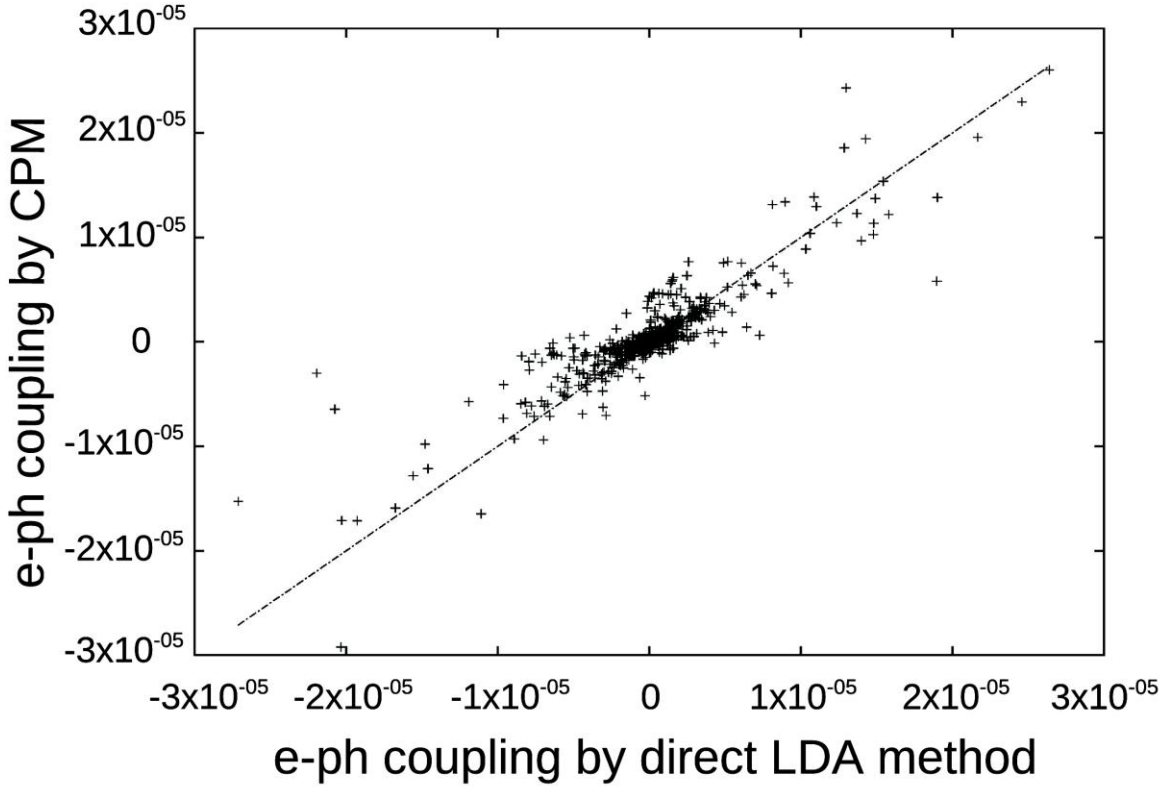

Figure S1: A comparison between the calculated electron-phonon couplings (in a.u.) for a few atomic displacements (near the center and near the surface) from the CPM and the direct DFT-LDA calculations.

(4) The quantum dot size scaling of the reorganization energy λ:

The calculated λ is plotted as a function of the inverse of the total number of atoms N in Figure S2. A straight line relationship is observed. Such scaling feature can be understood as the following. For each atomic movement, the electron-phonon coupling constant scales as $1/\Omega$, where Ω is the volume of the quantum dot. This is due to the normalization of the wave function ψ_i. For a harmonic oscillator with a spring constant of k, if an external force $C_{i,i}(\vec{R})$ is applied to this oscillator, the relaxation energy (reorganization energy) will be $-0.5C_{i,i}^2(\vec{R})/k \propto 1/\Omega^2$. Since the number of atoms is also proportional to Ω, the overall reorganization energy λ is proportional to $1/\Omega$.

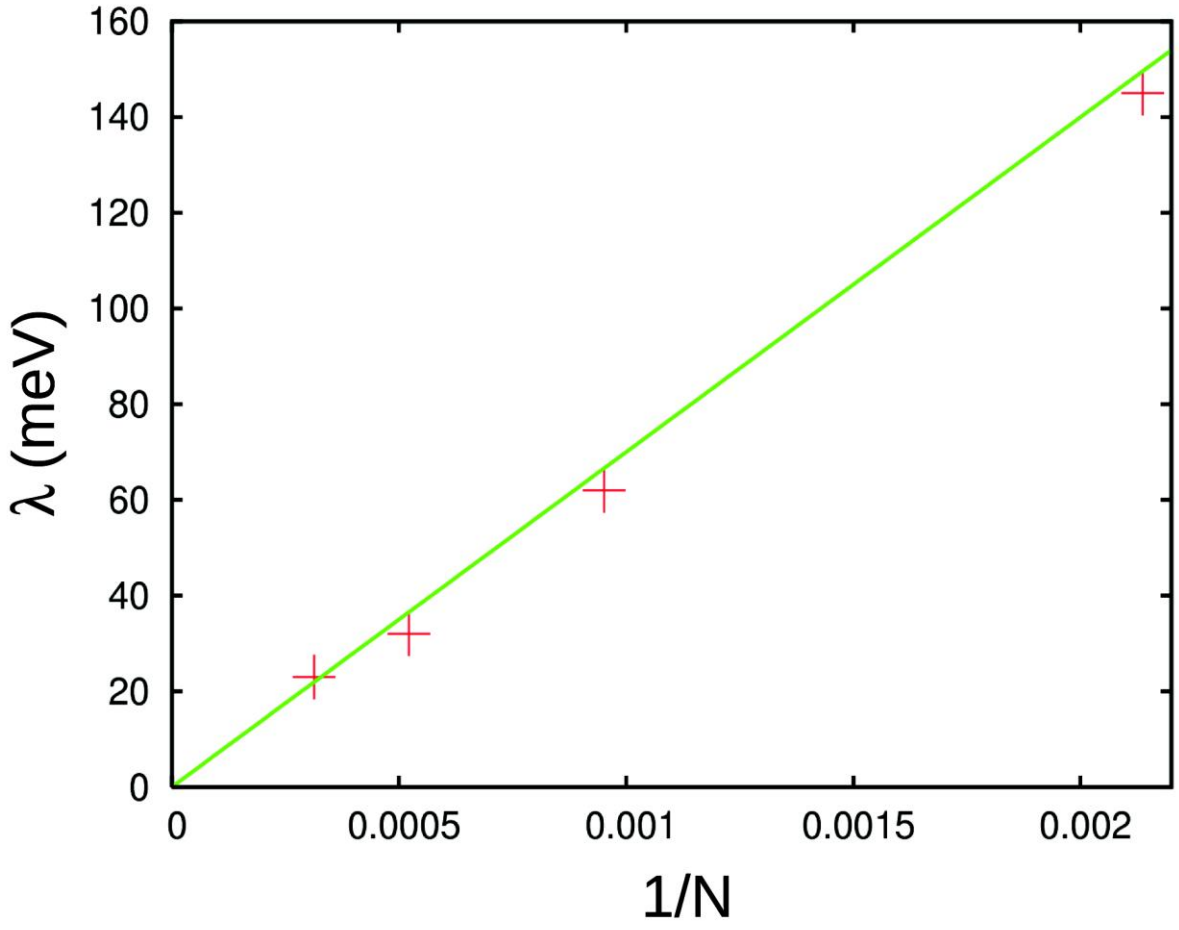

Figure S2: The calculated reorganization energies λ as a function of the inverse of the number of atoms ($1/N$). The green line indicates a linear fit.

(5) Local density of state calculations:

The generalized moment method (GMM)[11] is used to calculate the local density of states (LDOS) at the molecule Sn_2S_6. The results are shown in Figure S3, Figure S4 for the two different attachments, respectively. From the LDOS, one can see where the local states start to appear. Comparing that to the QD conduction band minimum (CBM), we can get the barrier height ΔE as shown in Figure 1(C). We found that such ΔE is about 2.4 eV for the large QDs. For the smaller QDs, this barrier height drops to ~1.8 eV due to quantum confinement effect of the CBM.

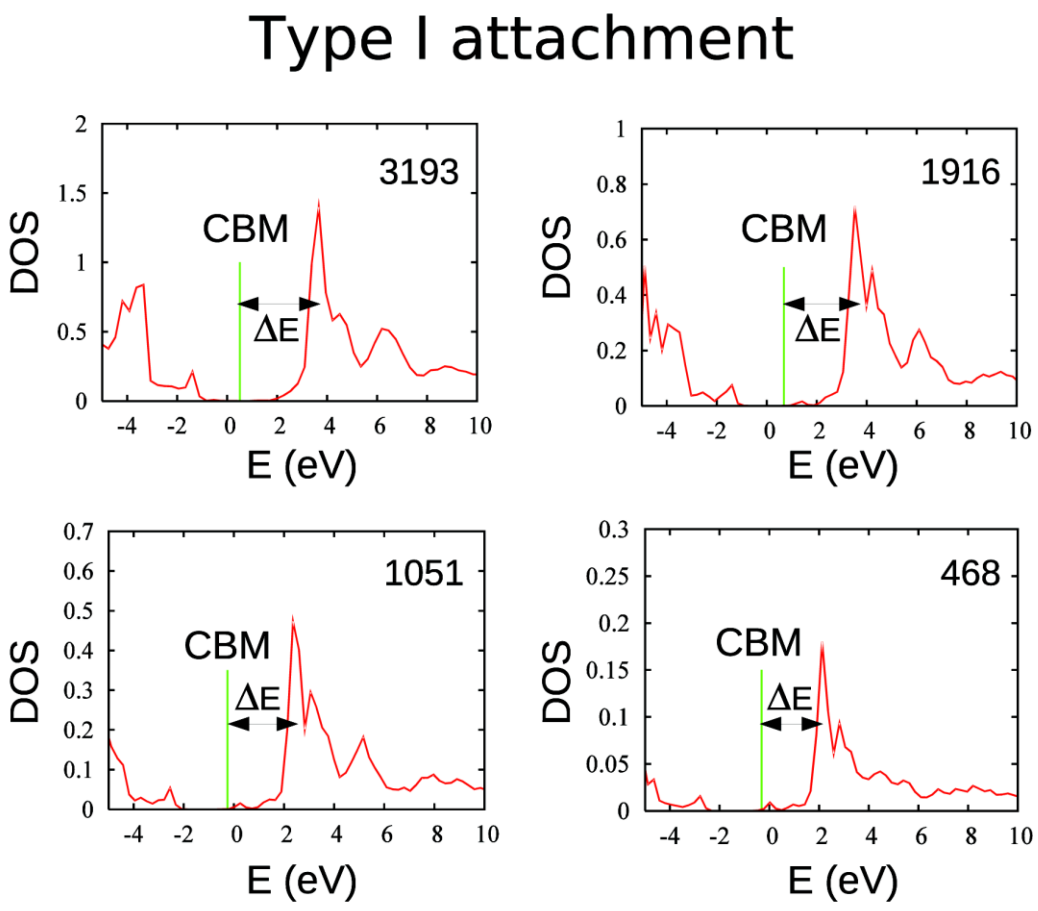

Figure S3: The local density of states at the molecule site for type I attachment. The eigen-energies of CBM for different QD sizes (the number of atoms is indicated in the top right corner of each panel) are shown by the green vertical lines. ΔE is the estimated barrier height in the over-the-barrier activation mechanism.

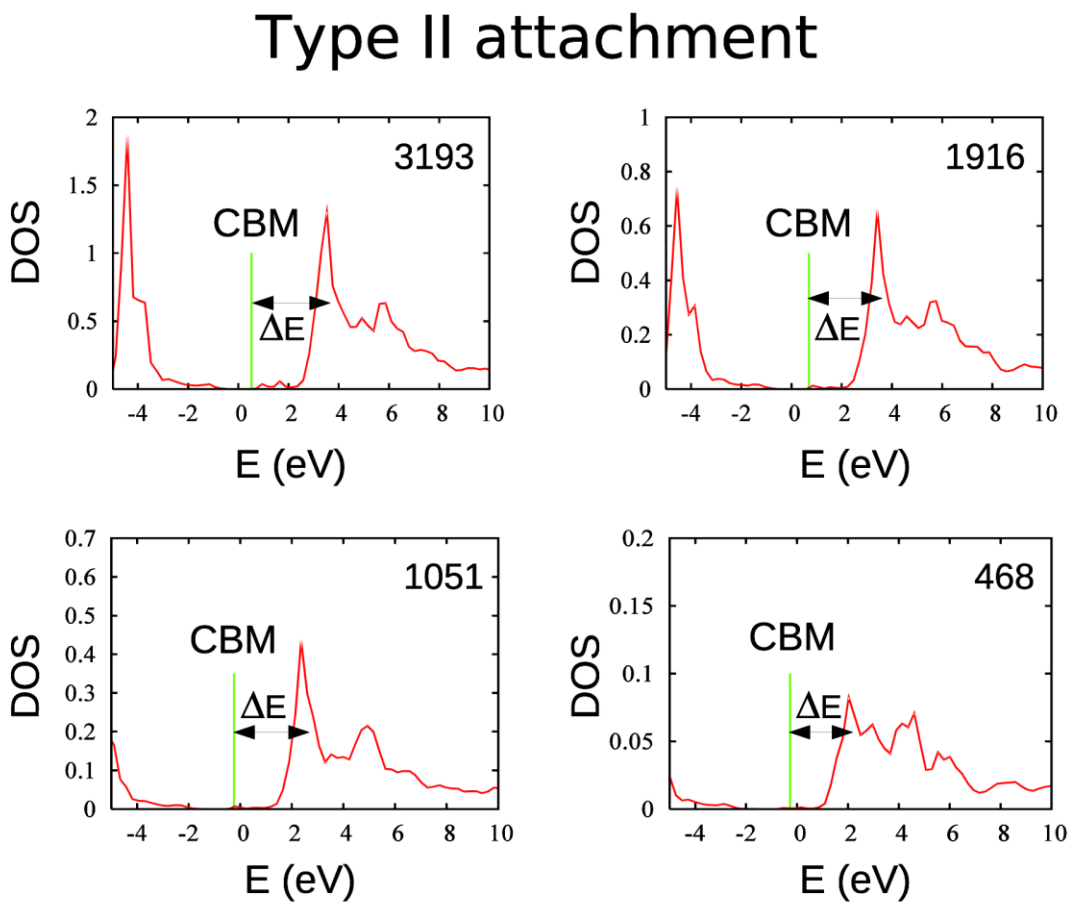

Figure S4: The local density of states at the molecule site for type II attachment. All the notations are the same as in Figure S3.

(6) Mobility calculation for the supercrystal:

With hopping rates between quantum dots at hand, one can calculate the electron mobility at low carrier density and low electric fields using the following procedure. Let τ_{ab}^{-1} be the hopping rate between two quantum dots *a* and *b*. It is known[12] that the electrical transport at low electric field and low carrier density is fully equivalent to the transport in a network of conductors where any two neighboring quantum dots have been connected with a conductance $G_{ab} = G_{ba} = e^2 n_a \tau_{ab}^{-1} / k_B T = e^2 n_b \tau_{ba}^{-1} / k_B T$ where n_a is the equilibrium occupation of state *a* given by the Boltzmann distribution, *e* is the elementary charge and k_B is the Boltzmann constant.

We construct the portion of the cubic supercrystal with $n_1 \times n_2 \times n_3$ quantum dots (of the size $L_x = L_y = L_z = L$), where $n_1 = n_2 = n_3 = 50$, i.e. a conductor network of the same dimensions. The equivalent conductance of such network is found by solving the linear equations for the potential of nodes in the circuit. These equations read $\sum_j (V_i - V_j) G_{ij} = 0$ where *j* is a neighbor of *i*. Periodic boundary conditions for V_i are applied in two directions (say *y* and *z*). For the *x* direction, we have $V_i = 0$ for the first *y*-*z* plane, and $V_i = U$ for the n_1-th *y*-*z* plane. A linear equation is then formed to solve for V_i in the interior planes. The current I_x through a plane perpendicular to the *x* direction is then calculated and the equivalent conductance is found as $G_x = I_x / U$. The mobility in *x*-direction is then given by $\mu_x = G_x / neL$, where *n* is the average concentration of carriers. Using the size fluctuation, we have randomly assigned the size, hence ε_i on each QD according to the fluctuation. We have calculated the G_{ab} using Eq.(2). To simulate the effects of loose attachment we have also multiplied G_{ab} with a random number uniformly distributed among 0 and 1.

References

1. Hohenberg, P.; Kohn, W. *Phys. Rev. B* **1964,** 136, (3B), B864.
2. Kohn, W.; Sham, L. J. *Phys. Rev.* **1965,** 140, (4A), 1133.
3. Perdew, J. P.; Zunger, A. *Phys. Rev. B* **1981,** 23, (10), 5048-5079.
4. Hafner, G. K. a. J. *Phys. Rev. B* **1993,** 47, (1), 558–561.
5. Kresse, G.; Furthmuller, J. *Phys. Rev. B* **1996,** 54, (16), 11169-11186.
6. Vanderbilt, D. *Phys. Rev. B* **1990,** 41, (11), 7892-7895.
7. Wang, L. W. *Phys. Rev. B* **2002,** 65, (15), 153410.
8. Vukmirovic, N.; Wang, L. W. *Nano Lett.* **2009,** 9, (12), 3996-4000.
9. Vukmirovic, N.; Wang, L. W. *Appl. Phys. Lett.* **2010,** 97, (4), 043305.
10. Vukmirovic, N.; Wang, L. W. *Phys. Rev. B* **2010,** 81, (3), 035210.
11. Wang, L. W. *Phys. Rev. B* **1994,** 49, (15), 10154-10158.
12. Ambegaokar, V.; Halperin, B. I.; Langer, J. S. *Phys. Rev. B* **1971,** 4, (8), 2612-2620.